Disrupting Transcriptional Feedback Yields an Escape-Resistant Antiviral

Sonali Chaturvedi[1], Marie Wolf[1], Joshua Glazier[1], Noam Vardi[1], Matilda F. Chan[2,3], Leor S. Weinberger[1,4,5*]

Affiliations:

[1]Gladstone|UCSF Center for Cell Circuitry, Gladstone Institutes, San Francisco, CA 94158;

[2]Francis I. Proctor Foundation,

[3]Department of Ophthalmology,

[4]Department of Biochemistry and Biophysics, and

[5]Department of Pharmaceutical Chemistry, University of California, San Francisco, CA 94158

*to whom correspondence should be addressed: leor.weinberger@gladstone.ucsf.edu

Abbreviations: circuit disrupting oligonucleotide therapy (C-DOT); human cytomegalovirus (CMV); herpes simplex virus type 1 (HSV-1)

Keywords: herpesvirus; autoregulatory circuit; transcriptional feedback; viral evolution; oligonucleotide therapy

Abstract: 222 words

Main Text: 1978 words

Figures: 4 (color)

Abstract:

From bacteria to cancers, it has long been recognized that drug-resistant mutants emerge quickly, causing significant morbidity and mortality[1-3]. Antiviral resistance in herpesviruses is of particular concern[4,5] with herpes simplex virus type 1 (HSV-1)—a leading cause of blindness—and human herpesvirus 5, cytomegalovirus (CMV)—a leading cause of birth defects and transplant failure—exhibiting substantial resistance to standard-of-care antivirals in the clinic[6,7]. Combination therapies, which limit resistance by necessitating multiple viral mutations, can be effective but increase the risk of off-target effects and associated toxicity and are absent for most viral diseases. Here, we present proof-of-concept for a novel approach that disrupts viral auto-regulatory circuits with a single molecule and limits resistance by requiring multiple viral mutations. We develop DNA-based circuit-disruptor oligonucleotide therapies (C-DOTs) that exploit this mechanism by interfering with transcriptional negative feedback in human herpesviruses (CMV and HSV-1) thereby increasing viral transcription factors to cytotoxic levels. C-DOTs reduce viral replication >100-fold, prevent emergence of resistant mutants in continuous culture, are effective in high-viremic conditions where existing antivirals are ineffective, and show efficacy in mice. Strikingly, no C-DOT-resistant mutants evolved in >60 days of culture, in contrast to approved herpesvirus antivirals where resistance rapidly evolved. Overall, the results demonstrate that oligonucleotide therapies targeting feedback circuits are escape resistant and could have broad therapeutic applicability to viruses, microbes, and neoplastic cells.

Main text:

The time to emergence of drug-resistant 'escape' mutants is typically estimated from the mutation rate, μ, and the effective population size, N[8,9]. Many viruses exhibit large μ such that frequency of mutants ($\mu \times N$) is >1, even for moderate virus population sizes (e.g., if $\mu \sim 10^{-5}$ then for $\mu \times N > 1$ requires only that $N > 10^5$). Herpesviruses, for example, exhibit high mutation rates[10,11], which may explain the substantial antiviral resistance observed in clinical settings[4,5]. In particular, herpes simplex virus type 1 (HSV-1)—a leading cause of blindness—exhibits resistance to acyclovir (ACV) in ~40% of transplant patients[6] while human herpesvirus 5, cytomegalovirus (CMV)—a leading cause of birth defects and transplant failure—exhibits resistance to ganciclovir (GCV) in 30–75% of patients[7]. ACV and GCV resistance arises because their antiviral activity requires herpesvirus thymidine kinase (TK), and single-base mutations destroy TK activity (with a $\mu \sim 10^{-3}$)[10] driving TK escape mutants within a single generation[12], which ultimately led to the development of non-TK drug targets[13,14]. Resistance to these new therapies is still being clinically evaluated, but, given the generality of resistance to antimicrobials[1-3], is likely unavoidable.

Combination therapy, wherein multiple drugs simultaneously inhibit different viral targets, is one approach used to limit antiviral resistance. For a two-drug therapy, escape mutants are predicted to arise at a rate $\sim\mu^2$ (i.e., the requirement for mutants to arise becomes $\mu^2 \cdot N > 1$), which requires substantially larger virus populations (i.e., $N > \mu^{-2}$). However, each constituent antiviral must have a distinct molecular target, as well as favorable toxicity, efficacy, bioavailability, and dosing profiles. These criteria can be challenging to satisfy and such targets are still being characterized for herpesviruses. One proposed alternative has been to mimic the evolutionary benefits of combination therapy by inhibiting protein-protein or protein-DNA interactions with a single molecule; this has remained technically challenging but transcriptional auto-regulatory (feedback) circuits present an attractive target for this approach[15]. Both CMV and HSV-1 utilize transcriptional feedback to regulate immediate-early (IE) viral gene expression, which is obligate to transactivate downstream viral genes, ultimately licensing virus maturation[16-19]. In CMV, the 86-kDa immediate early (IE86; a.k.a. IE2) protein, and in HSV-1 the IE175 (a.k.a. ICP4) protein, are indispensable transcriptional transactivators[20,21]. Critically, IE86 and IE175 are cytotoxic when expression is misregulated above tightly auto-regulated homeostatic levels, and both CMV

and HSV-1 encode negative-feedback circuits to maintain IE86 and IE175 levels below their respective cytotoxic thresholds[20,22]. These feedback circuits are comprised of a protein-DNA interaction wherein the IE protein binds to a 14–15 bp palindromic cis-repression sequence (crs) within its respective promoter and auto-represses its own transcription (Fig. 1a). Disrupting this feedback by altering the crs increases IE protein levels to cytotoxic levels, leading to a >100-fold reduction in viral replication[22,23].

We hypothesized that oligonucleotides mimicking the palindromic DNA-binding site could titrate IE proteins away from the crs and act as competitive inhibitors to disrupt IE negative feedback (Fig. 1a). Mathematical modeling predicted that such circuit-disrupting oligonucleotide therapies (C-DOTs) may in fact raise IE protein to cytotoxic levels (Fig. 1b and Extended Data Fig. 1a). Theoretically, to escape C-DOTs and recapitulate a feedback loop, the virus would need to evolve a new IE-protein domain to recognize a new DNA sequence and *simultaneously* evolve a new cognate DNA binding sequence in the IE promoter; these C-DOT escape mutants would evolve on order of μ^2, which would occur substantially slower than observed for ACV/GCV resistance (Fig. 1c). It is conceivable that single mutants in the IE protein could arise and bind alternate crs-like sequences pre-existing in the promoter region, thereby circumventing the combinatorial mutation hypothesis. However, there are no comparable palindromes within 500 bp of the MIEP promoter and if such sequences were present, then crs-deletion mutants should strongly select for such IE86 mutants that can recapitulate negative feedback, which does not occur over ~1 month of culturing[22].

To find oligonucleotides that optimally titrate IE proteins, we developed an *in vitro* liquid-chromatography assay to quantify the efficiency of various linear DNA oligonucleotides in catalyzing formation of the IE86 protein-DNA complex (Fig. 2a). To validate the assay, we used electrophoretic mobility shift assays (EMSA) and verified that purified IE86 protein bound double-stranded DNA oligonucleotides in a sequence-specific manner (Extended Data Fig. 1b). We tested an array of crs-encoding oligonucleotides of various lengths and found a linear 28 base-pair (bp) DNA most efficiently catalyzed formation of the IE86-DNA complex (Fig. 2b–c). Shorter or

longer crs-encoding DNAs were less efficient at titrating IE86 and promoting protein-DNA complex formation.

To test if these DNAs disrupted negative feedback, we used a retinal pigment epithelial cell line stably transduced with a previously described minimal IE86 negative-feedback reporter circuit[22]. These cells express the IE86 and GFP under the control of the IE86 promoter-enhancer such that increases in GFP indicate disruption of negative-feedback leading to cell death 48–72 hours later (Fig. 2d). Cells were nucleofected with the putative C-DOTs, or sequence-scrambled control oligonucleotides, and GFP expression assayed by flow cytometry at 48 h (Fig. 2d). DNA uptake by cells was verified by cy3 fluorescence (Extended Data Fig. 1c) and to enhance oligonucleotide stability, DNAs were modified by internal phosphorothioate bonds (Extended Data Fig. 1d). In agreement with the biochemical assays, the 28bp DNA most efficiently increased the GFP+ population (Fig. 2e) and correspondingly decreased live-cell percentages (Fig. 2f). Feedback-circuit disruption was dose dependent (Extended Data Fig. 2a-b) and was enhanced by concatemerization as well as using nanoparticles to enhance cell uptake (Extended Data Fig. 3a-c). Collectively, these results indicated that relatively short (< 30bp) double-stranded DNAs might be viable circuit disruptor oligonucleotides.

Next, we investigated the effects of disrupting transcriptional feedback in the context of viral infection. We designated the 28bp DNA for CMV IE86 as C-DOT^{C} (C-DOT for CMV) and found that C-DOT^{C} efficiently disrupted IE86 negative feedback in cells infected with a clinically-derived isolate of CMV[24] (Fig. 3a). We next hypothesized that replacing the 14bp crs within C-DOT^{C} with the 15bp repression sequence from IE175's promoter could generate a C-DOT for HSV-1 (now termed C-DOT^{H}). As predicted, C-DOT^{H} disrupted IE175 negative feedback in cells infected with clinically-derived HSV-1[25] (Fig. 3b). There was minimal difference in %IE positive cells, indicating that C-DOTs did not alter permissiveness of cells to viral infection (Extended Data Fig. 2c). Strikingly, the C-DOTs also reduced single-round viral replication titers for both CMV and HSV-1 at multiplicity of infection (MOI) of 0.1 by ~100 fold (Fig. 3c–d), in agreement with genetic disruption of IE negative feedback[22]. To be sure that the observed antiviral effects were not specific to the virus strain or cell type used, we also tested (i) CMV strain AD169 and (ii)

various GCV-resistant CMV strains in human foreskin fibroblasts, as well as (iii) murine CMV and (iv) rhesus CMV, in mouse and primate cells respectively, and in all cases found similar 100-fold titer reduction using the corresponding C-DOTs (Extended Data Fig. 4a-c).

In stark contrast to ACV and GCV, C-DOT increases virus fold reduction at higher MOI, and, at MOI = 2, C-DOTs exhibited a > 1300x reduction whereas ACV/GCV elicited 35–70x reduction in viral replication (Fig. 3c–d). Such robustness to high-viremic conditions has not been previously described for an antiviral[26], but is consistent with the putative C-DOT mechanism of action through feedback disruption and IE-mediated cytotoxicity—higher MOIs deliver more genomes, which generates more potentially cytotoxic IE protein.

Importantly, sequence-scrambled oligonucleotides (C-DOT^{Scram}) did not exhibit antiviral effects suggesting that C-DOTs are not acting via innate-immune mechanisms (e.g., activation of cGAS-STING pathway via TLR9), which is consistent with efficient cGAS pathway activation requiring DNAs of > 300bp[27], whereas C-DOTs are < 30bp. However, to verify that C-DOT activity is independent of cGAS-STING, we tested C-DOTs under conditions of high and low cGAS-STING expression and observed little difference in C-DOT antiviral effects and no effects for C-DOT^{Scram} in either setting (Extended Data Fig. 5b). Moreover, C-DOTs did not activate TLR9 expression (Extended Data Fig. 5a).

Next, to examine the rate of emergence of viral escape mutants, we used a continuous-culture approach where virus was consecutively passaged from infected cells to fresh uninfected cells every 4 days (a typical CMV replication round) until virus was undetectable in presence of C-DOT treatment (~40–60 days; Fig. 3e). C-DOT^{C} was compared to Fomivirsen[28], the first approved DNA oligonucleotide therapy (an anti-sense DNA for IE86); C-DOT^{H} was compared with ACV. As previously reported[12], we found HSV-1 resistance to ACV emerges within two rounds of infection (Extended Data Fig. 5f) and that CMV resistance to Fomivirsen[28] arises within 3-4 rounds of infection (Extended Data Fig. 5d-e).

In striking contrast, C-DOT^{C} steadily reduced CMV titers to below the limit of detection by day 52, with no evidence of CMV resistance to the C-DOT^{C} (Fig. 3f). Subsequent sub-culturing showed that the virus was cleared (Extended Data Fig. 5c). Similarly, C-DOT^{H} steadily reduced HSV-1 titers to below detection by day 40, with no evidence of resistance (Fig. 3g). In agreement with this, sequence analysis indicated that no virus mutations arose in the 500bp-region surrounding the promoter repression sequences (Extended Data Fig. 6) and only single-nucleotide transient polymorphisms in the IE-protein regions responsible for DNA binding (Extended Data Fig. 7). Overall, these results indicate that disrupting feedback may be an escape-resistant antiviral strategy.

Finally, we tested if transcriptional feedback could be disrupted *in vivo* using the established model of herpes infection in mice[29]. Briefly, in this model, mice are infected with HSV-1 in the cornea, and interventions are topically applied at the site of infection to test efficacy. Using standard practice, we infected mice with HSV-1 IE175-YFP, then 6 hours later (to avoid interfering with virus uptake), oligonucleotides were applied and after two days, corneas were harvested for imaging and quantification of viral replication by q-PCR and titering (Fig. 4a). C-DOT uptake by cells was quantified by Cy3 fluorescence (Extended Data Fig. 8a) and as predicted, C-DOT treatment first caused an increase in IE175 (Extended Data Fig. 8b) followed by a significant reduction in the percentage of HSV-1 infected cells (Fig. 4b–c). In agreement with these data, C-DOT^{H} treatment reduced viral titer by 150-fold (Fig. 4d) and significantly reduced viral genome replication (Fig. 4e). Together, these results demonstrate that feedback disruption reduces viral replication *in vivo*.

Overall, these results indicate that transcriptional feedback could represent a new antiviral target with the potential to substantially delay the emergence of resistance (Fig. 3) and overcome significant treatment barriers including the reduction-in-efficacy at high-viremic loads[26]. In general, oligonucleotide therapies offer specificity with the potential for fewer off target effects over small molecules. While delivery of oligonucleotides remains a major challenge, significant clinical advances have been made with the recent FDA approval of antisense and exon-skipping oligonucleotide therapies delivered via nanoparticles[30-32]. Therefore, we also tested C-DOTs using

nanoparticle carriers, in the absence of transfection, and found similar antiviral effects (Extended Data Fig. 9a-b). One could envision nanoparticles harboring combinatorial C-DOTs to treat infections of unknown etiology—a significant problem for ocular infections[33,34]—and our data indicate that such combinatorial 'multiplexed' C-DOTs may be feasible (Extended Data Fig. 9c-d).

From the perspective of resistance, disrupting autoregulatory circuits yields several theoretical advantages and our calculations represent a lower limit for the time to escape from feedback disruptors. Regulatory loci typically have lower genetic variability than enzymes or receptors[10,35] so mutants in the promoter region and reading frame will arise relatively slowly. Second, > 2 mutations will likely be required for generating new DNA-recognition domains in proteins; for herpesviruses even assuming that the regulatory region mutates with average viral frequency[10,35] (it is in fact lower) translates to the escape rate scaling as $\sim 10^{-4n}$ (where $n > 2$). Furthermore, putative escape mutants, if they are generated, would have a relative fitness roughly equivalent to wild type, so their selection coefficient and pre-existing abundance will be low. As such, we predict that feedback circuit disruption may be an attractive target in other viruses, microbes, and in neoplastic cells with aberrant auto-regulatory circuits.

References:

1 Meylan, S., Andrews, I. W. & Collins, J. J. Targeting Antibiotic Tolerance, Pathogen by Pathogen. *Cell* **172**, 1228-1238, doi:10.1016/j.cell.2018.01.037 (2018).

2 Lee, H. H., Molla, M. N., Cantor, C. R. & Collins, J. J. Bacterial charity work leads to population-wide resistance. *Nature* **467**, 82-85, doi:10.1038/nature09354 (2010).

3 Goldberg, D. E., Siliciano, R. F. & Jacobs, W. R., Jr. Outwitting evolution: fighting drug-resistant TB, malaria, and HIV. *Cell* **148**, 1271-1283, doi:10.1016/j.cell.2012.02.021 S0092-8674(12)00221-8 [pii] (2012).

4 Piret, J. & Boivin, G. Antiviral drug resistance in herpesviruses other than cytomegalovirus. *Rev Med Virol* **24**, 186-218, doi:10.1002/rmv.1787 (2014).

5 Lurain, N. S. & Chou, S. Antiviral drug resistance of human cytomegalovirus. *Clin Microbiol Rev* **23**, 689-712, doi:10.1128/CMR.00009-10 23/4/689 [pii] (2010).

6 Frobert, E. *et al*. Resistance of herpes simplex viruses to acyclovir: an update from a ten-year survey in France. *Antiviral Res* **111**, 36-41, doi:10.1016/j.antiviral.2014.08.013 (2014).

7 Emery, V. C. & Griffiths, P. D. Prediction of cytomegalovirus load and resistance patterns after antiviral chemotherapy. *Proc Natl Acad Sci U S A* **97**, 8039-8044, doi:10.1073/pnas.140123497 (2000).

8 Perelson, A. S. Modelling viral and immune system dynamics. *Nat Rev Immunol* **2**, 28-36, doi:10.1038/nri700 (2002).

9 Coffin, J. M. HIV population dynamics in vivo: implications for genetic variation, pathogenesis, and therapy. *Science* **267**, 483-489 (1995).

10 Lu, Q., Hwang, Y. T. & Hwang, C. B. Mutation spectra of herpes simplex virus type 1 thymidine kinase mutants. *J Virol* **76**, 5822-5828 (2002).

11 Renzette, N., Bhattacharjee, B., Jensen, J. D., Gibson, L. & Kowalik, T. F. Extensive genome-wide variability of human cytomegalovirus in congenitally infected infants. *PLoS Pathog* **7**, e1001344, doi:10.1371/journal.ppat.1001344 (2011).

12 Coen, D. M. & Schaffer, P. A. Two distinct loci confer resistance to acycloguanosine in herpes simplex virus type 1. *Proc Natl Acad Sci U S A* **77**, 2265-2269 (1980).

13 Goldner, T. *et al*. The novel anticytomegalovirus compound AIC246 (Letermovir) inhibits human cytomegalovirus replication through a specific antiviral mechanism that involves the viral terminase. *J Virol* **85**, 10884-10893, doi:10.1128/JVI.05265-11 (2011).

14 Jaishankar, D. *et al*. An off-target effect of BX795 blocks herpes simplex virus type 1 infection of the eye. *Sci Transl Med* **10**, doi:10.1126/scitranslmed.aan5861 (2018).

15 Pai, A. & Weinberger, L. S. Fate-Regulating Circuits in Viruses: From Discovery to New Therapy Targets. *Annu Rev Virol* **4**, 469-490, doi:10.1146/annurev-virology-110615-035606 (2017).

16 Enquist, L. W. & Leib, D. A. Intrinsic and Innate Defenses of Neurons: Detente with the Herpesviruses. *J Virol* **91**, doi:10.1128/JVI.01200-16 (2017).

17 Weller, S. K. & Coen, D. M. Herpes simplex viruses: mechanisms of DNA replication. *Cold Spring Harb Perspect Biol* **4**, a013011, doi:10.1101/cshperspect.a013011 (2012).

18 Shenk, T. E. & Stinski, M. F. Human cytomegalovirus. Preface. *Curr Top Microbiol Immunol* **325**, v (2008).

19 Mocarski, E. S., Shenk, T. & Pass, R. F. in *Fields' virology* (ed David M. Knipe) 2708-2772 (Lippincott Williams & Wilkins, 2006).

20 Liu, B., Hermiston, T. W. & Stinski, M. F. A cis-acting element in the major immediate-early (IE) promoter of human cytomegalovirus is required for negative regulation by IE2. *J Virol* **65**, 897-903 (1991).

21 Paterson, T. & Everett, R. D. The regions of the herpes simplex virus type 1 immediate early protein Vmw175 required for site specific DNA binding closely correspond to those involved in transcriptional regulation. *Nucleic Acids Res* **16**, 11005-11025 (1988).

22 Teng, M. W. *et al*. An endogenous accelerator for viral gene expression confers a fitness advantage. *Cell* **151**, 1569-1580, doi:10.1016/j.cell.2012.11.051 (2012).

23 Isomura, H. *et al*. A cis element between the TATA Box and the transcription start site of the major immediate-early promoter of human cytomegalovirus determines efficiency of viral replication. *J Virol* **82**, 849-858, doi:10.1128/JVI.01593-07 (2008).

24 Vardi, N., Chaturvedi, S. & Weinberger, L. S. Feedback-mediated signal conversion promotes viral fitness. *Proc Natl Acad Sci U S A* **115**, E8803-E8810, doi:10.1073/pnas.1802905115 (2018).

25 Everett, R. D., Murray, J., Orr, A. & Preston, C. M. Herpes simplex virus type 1 genomes are associated with ND10 nuclear substructures in quiescently infected human fibroblasts. *J Virol* **81**, 10991-11004, doi:10.1128/JVI.00705-07 (2007).

26 Asberg, A. *et al*. Lessons Learned From a Randomized Study of Oral Valganciclovir Versus Parenteral Ganciclovir Treatment of Cytomegalovirus Disease in Solid Organ Transplant Recipients: The VICTOR Trial. *Clin Infect Dis* **62**, 1154-1160, doi:10.1093/cid/ciw084 (2016).

27 Luecke, S. *et al*. cGAS is activated by DNA in a length-dependent manner. *EMBO Rep* **18**, 1707-1715, doi:10.15252/embr.201744017 (2017).

28 Mulamba, G. B., Hu, A., Azad, R. F., Anderson, K. P. & Coen, D. M. Human cytomegalovirus mutant with sequence-dependent resistance to the phosphorothioate oligonucleotide fomivirsen (ISIS 2922). *Antimicrob Agents Chemother* **42**, 971-973 (1998).

29 Lahmidi, S., Yousefi, M., Dridi, S., Duplay, P. & Pearson, A. Dok-1 and Dok-2 Are Required To Maintain Herpes Simplex Virus 1-Specific CD8(+) T Cells in a Murine Model of Ocular Infection. *J Virol* **91**, doi:10.1128/JVI.02297-16 (2017).

30 Adams, D. *et al*. Patisiran, an RNAi Therapeutic, for Hereditary Transthyretin Amyloidosis. *N Engl J Med* **379**, 11-21, doi:10.1056/NEJMoa1716153 (2018).

31 Kanasty, R., Dorkin, J. R., Vegas, A. & Anderson, D. Delivery materials for siRNA therapeutics. *Nat Mater* **12**, 967-977, doi:10.1038/nmat3765 (2013).

32 Khvorova, A. & Watts, J. K. The chemical evolution of oligonucleotide therapies of clinical utility. *Nat Biotechnol* **35**, 238-248, doi:10.1038/nbt.3765 (2017).

33 Cunningham, E. T. Cytomegalovirus: ophthalmic perspectives on a pervasive pathogen. *Expert Review of Ophthalmology* **6**, 489-491, doi:10.1586/eop.11.50 (2011).

34 Elia, M. H., J.J., and Gaudio, P.A. in *EyeNet Magazine* 37-38 (2016).

35 Renzette, N. *et al*. Limits and patterns of cytomegalovirus genomic diversity in humans. *Proc Natl Acad Sci U S A* **112**, E4120-4128, doi:10.1073/pnas.1501880112 1501880112 [pii] (2015).

36. M. P. Macias, M. F. Stinski, An in vitro system for human cytomegalovirus immediate early 2 protein (IE2)-mediated site-dependent repression of transcription and direct binding of IE2 to the major immediate early promoter. *Proc Natl Acad Sci U S A* **90**, 707-711 (1993).

37. P. J. Morley, P. Ertl, C. Sweet, Immunisation of Balb/c mice with severely attenuated murine cytomegalovirus mutants induces protective cellular and humoral immunity. *J Med Virol* **67**, 187-199 (2002).

38. W. L. Chang, P. A. Barry, Cloning of the full-length rhesus cytomegalovirus genome as an infectious and self-excisable bacterial artificial chromosome for analysis of viral pathogenesis. *J Virol* **77**, 5073-5083 (2003).

39. R. D. Everett, G. Sourvinos, A. Orr, Recruitment of herpes simplex virus type 1 transcriptional regulatory protein ICP4 into foci juxtaposed to ND10 in live, infected cells. *J Virol* **77**, 3680-3689 (2003).

40. S. M. Brown, D. A. Ritchie, J. H. Subak-Sharpe, Genetic studies with herpes simplex virus type 1. The isolation of temperature-sensitive mutants, their arrangement into complementation groups and recombination analysis leading to a linkage map. *J Gen Virol* **18**, 329-346 (1973).

41. L. J. Reed, & Muench, H. , A simple method of estimating fifty percent endpoints. *Am. J. Hygiene* **27**, 493-497 (1938).

42. M. F. Chan, Z. Werb, Animal Models of Corneal Injury. *Bio Protoc* **5**, e1516 (2015).

43. N. L. Rosi *et al*., Oligonucleotide-modified gold nanoparticles for intracellular gene regulation. *Science* **312**, 1027-1030 (2006).

44. M. K. Skouboe *et al*., STING agonists enable antiviral cross-talk between human cells and confer protection against genital herpes in mice. *PLoS Pathog* **14**, e1006976 (2018).

Acknowledgments: We dedicate the manuscript to the memory of Cynthia Bolovan-Fritts who provided extensive technical support and made this work possible. We acknowledge Ariel Weinberger and Raghav Singhal for their input in modeling the ACV/GCV resistance. We thank Lewis Lanier, Peter Barry and Roger Everett for providing MCMV strain K181, Rhesus CMV 68.1 EGFP, HSV-1 17syn+ IE175-YFP virus. We thank Elena Ingerman, Melanie Ott, JJ Miranda, Siyu Zheng, Marielle Cavrois, Nandhini Raman, Elizabeth Tanner and the Weinberger lab for discussions and suggestions. We thank Kathryn Claiborn for reviewing the manuscript. We acknowledge Gladstone Flow Cytometry Core, funded through NIH P30 AI027763.
M.F.C. acknowledges National Institutes of Health (R01 EY022739), Research to Prevent Blindness (RPB Physician-Scientist Award to M.F.C and RPB Unrestricted Grant to the UCSF Department of Ophthalmology), and That Man May See Research Grant. This work was supported by the Bowes Distinguished Professorship, the Alfred P. Sloan Research Fellowship, the Pew Scholars in the Biomedical Sciences Program, NIH Director's New Innovator Award OD006677 and Pioneer Award OD17181 programs (to L.S.W.).

Author contributions: S.C. and L.S.W. conceived and designed the study. S.C., M.W., and M.F.C., designed and performed the experiments, and curated the data. N.V. and L.S.W. performed the mathematical modeling. S.C., M.W. and L.S.W. wrote the paper.

Author information:

Competing interests: L.S.W. is an inventor of "Compositions and methods of use thereof for identifying anti-viral agents" (US patent no. US10106817B2) and is a co-founder and chair of the Scientific Advisory Board of Autonomous Therapeutics Inc.

Correspondence and requests for materials should be addressed to leor.weinberger@gladstone.ucsf.edu

<u>Figure 1</u>: Theory predicts that antiviral disruption of transcriptional feedback would substantially delay evolution of resistance. (a) Schematics of the herpesvirus IE (IE86 and IE175) transcriptional negative-feedback circuits in the intact wild-type form (upper) and after disruption (lower) by putative circuit-disrupting oligonucleotide therapy (C-DOT). When feedback is intact, IE proteins bind the cis repression DNA sequence in their respective IE promoters (cyan) and downregulate transcriptional activity to prevent IE protein levels from reaching cytotoxic levels. When feedback is disrupted, for example by IE proteins being titrated away by binding free oligonucleotides encoding cis-repression sequences, IE promoter activity is not downregulated and IE proteins reach cytotoxic levels (~1.5-fold above homeostatic levels)[22]. (b) Numerical solutions of an experimentally validated computational model of IE feedback[22,24] showing that C-DOTs effectively break feedback to increase IE protein levels into the cytotoxic regime. See also Extended Data Fig. 1a. (c) Analytical calculation for the 50% emergence time of resistance mutants ($\tau_{resistance}$) as a function of the mutation rate μ. The observed emergence of resistance to GCV in the clinic[7] is shown as a point above the measured TK mutation rate ($\mu = 10^{-4}$). Putative C-DOT resistance, predicted to require at least two mutations (one in the protein and one in the promoter), is shown as a line corresponding to measured μ[11]. Inset: representative dynamics of emergence for either a GCV mutant (black) or a putative C-DOT mutant (cyan) that requires only viral two mutations. See Methods for equations.

Figure 1 (Chaturvedi et.al)

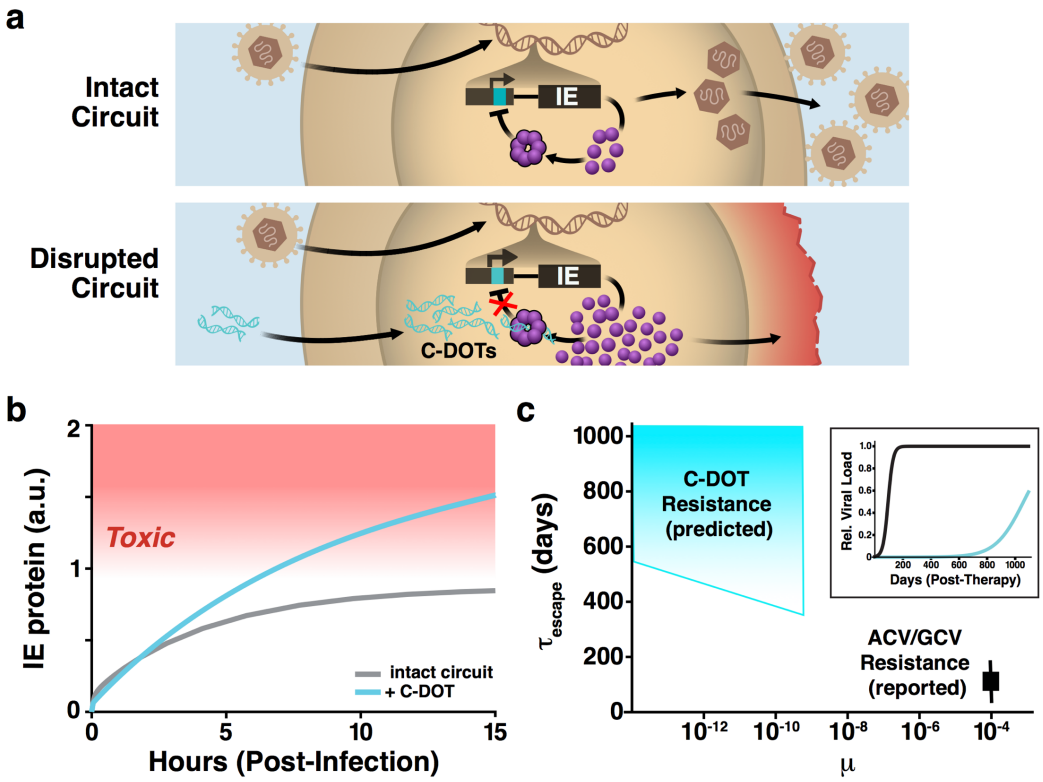

<u>Figure 2</u>: Biochemical and *in vitro* analyses identify oligonucleotides that disrupt transcriptional feedback circuitry. (a) Schematic of the IE86-protein binding assay: the C-terminus of the IE86 protein was expressed in *E. coli*, concentrated and incubated with 14–64bp DNA oligonucleotides for 30 minutes at room temperature, then passed through an FPLC column. Protein-DNA complex formation was quantified by optical density (OD 280nm) of FPLC fractions; the IE86 protein (obligate dimer) fragment elutes in the 15mL fraction, free dsDNA oligonucleotides elute in the 18mL fraction, and the multimeric protein-DNA complex elutes in the 13mL fraction. (b) FPLC chromatography profiles of IE86 protein fragment input and dsDNA input prior to co-incubation. (c) Chromatographs of IE86 fragment incubated with either a sequence-scrambled control dsDNA oligonucleotides or crs-containing dsDNA oligonucleotides of differential lengths. The 28bp crs DNA oligonucleotide most efficiently titrates free protein from the 15mL fraction into the 13mL fraction (~98% of protein is found in the 13mL protein-DNA complex fraction when the 28bp crs DNA oligonucleotide is added). (d) Left: Schematic of the minimal IE negative-feedback circuit (MIEP-IE86-IRES-GFP) encoded within the feedback-reporter cell line. Disruption of negative feedback generates increases in GFP fluorescence. Right: Flow cytometry of feedback reporter cells 48 h after nucleofection with either a 28bp crs-containing DNA oligonucleotide, a scrambled DNA oligonucleotide (negative control), or mock nucleofection (no DNA oligonucleotide) showing that crs-encoding DNA oligonucleotides disrupt feedback and act as a putative C-DOTs. (e, f) The 28bp crs-containing DNA oligonucleotide optimally disrupts feedback and induces cytotoxicity in the feedback-reporter cell line. DNA oligonucleotides (from the FPLC analysis in panel c above) were nucleofected into the reporter cell line and analyzed by flow cytometry after 48 h to determine IE86 expression (GFP; panel e), and cytotoxicity (panel f). (p-value less than 0.05 was considered statistically significant: *<0.05, **<0.01, ***<0.001, ****<0.0001).

Figure 2 (Chaturvedi et.al)

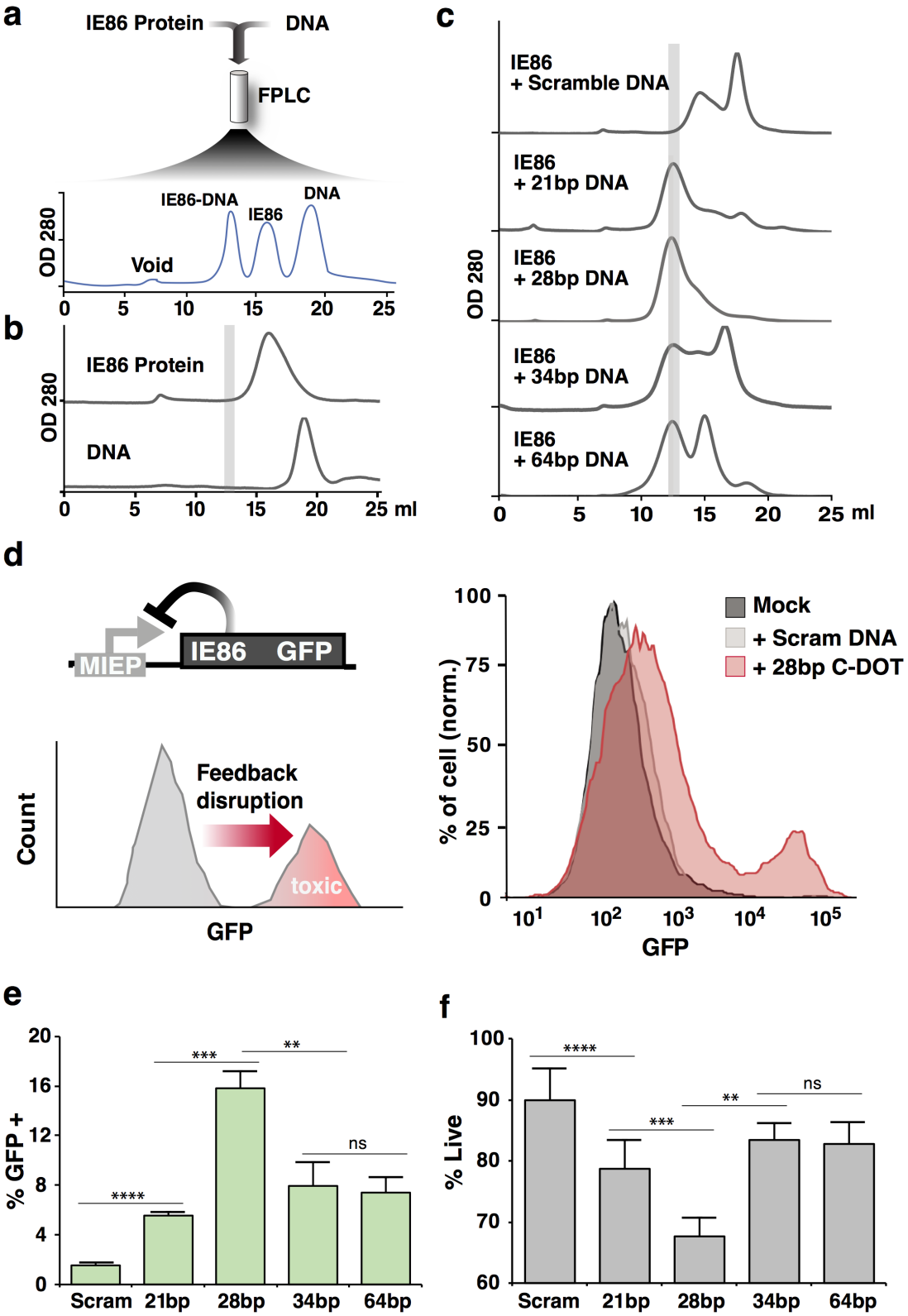

<u>Figure 3</u>: Feedback circuit disruption interferes with viral replication even at high MOI and limits the evolution of resistance. (a) Flow cytometry of ARPE-19 cells nucleofected with the 28bp dsDNA that titrates IE86 (C-DOT^{C}) or scrambled dsDNA sequence (C-DOT^{Scram}) and infected with a clinically derived CMV (TB40E) encoding an IE86-YFP (MOI = 0.1) then analyzed at 2 days post infection (dpi). (b) Flow cytometry of ARPE-19 cells nucleofected with a 29bp DNA to titrate IE175 (C-DOT^{H}) or scrambled dsDNA sequence (C-DOT^{Scram}) and infected with HSV-1 (17syn+ strain) encoding an IE175-YFP (MOI = 0.1) then analyzed at 2 dpi. (c) Single-round viral titering of CMV in the presence of 100μM GCV, PBS, or 25μM C-DOT^{C} (or C-DOT^{Scram}) at 4-days post infection under different initial MOIs. (d) Single-round viral titering of HSV-1 in presence of 100μM ACV or 25μM C-DOT^{H} (or C-DOT^{Scram}) at 4-days post infection under different HSV-1 MOIs. (e) Schematic of the continuous-culture experiment; ARPE-19 cells (+/- C-DOT) were infected with CMV or HSV-1 (0.1 MOI) and at 4-day post infection, supernatant was collected and was used to infect naïve ARPE-19 cells +/- C-DOT until day 60. (f) Continuous culture titers for CMV (TB40E-IE86-YFP) in the presence of C-DOT^{C} (red) or mock treatment (black). Fomivirsen resistance (positive slope of the titering dynamics) was observed beginning at day 12 (Extended Data Fig. 5d,e). (g) Continuous culture for HSV-1 (17syn+ IE175-YFP virus) in the presence of C-DOT^{H} (red) or mock treatment (black). ACV resistance (positive slope of the titering dynamics) observed beginning at day 4 (Extended Data Fig. 5f).

Figure 3 (Chaturvedi et al.)

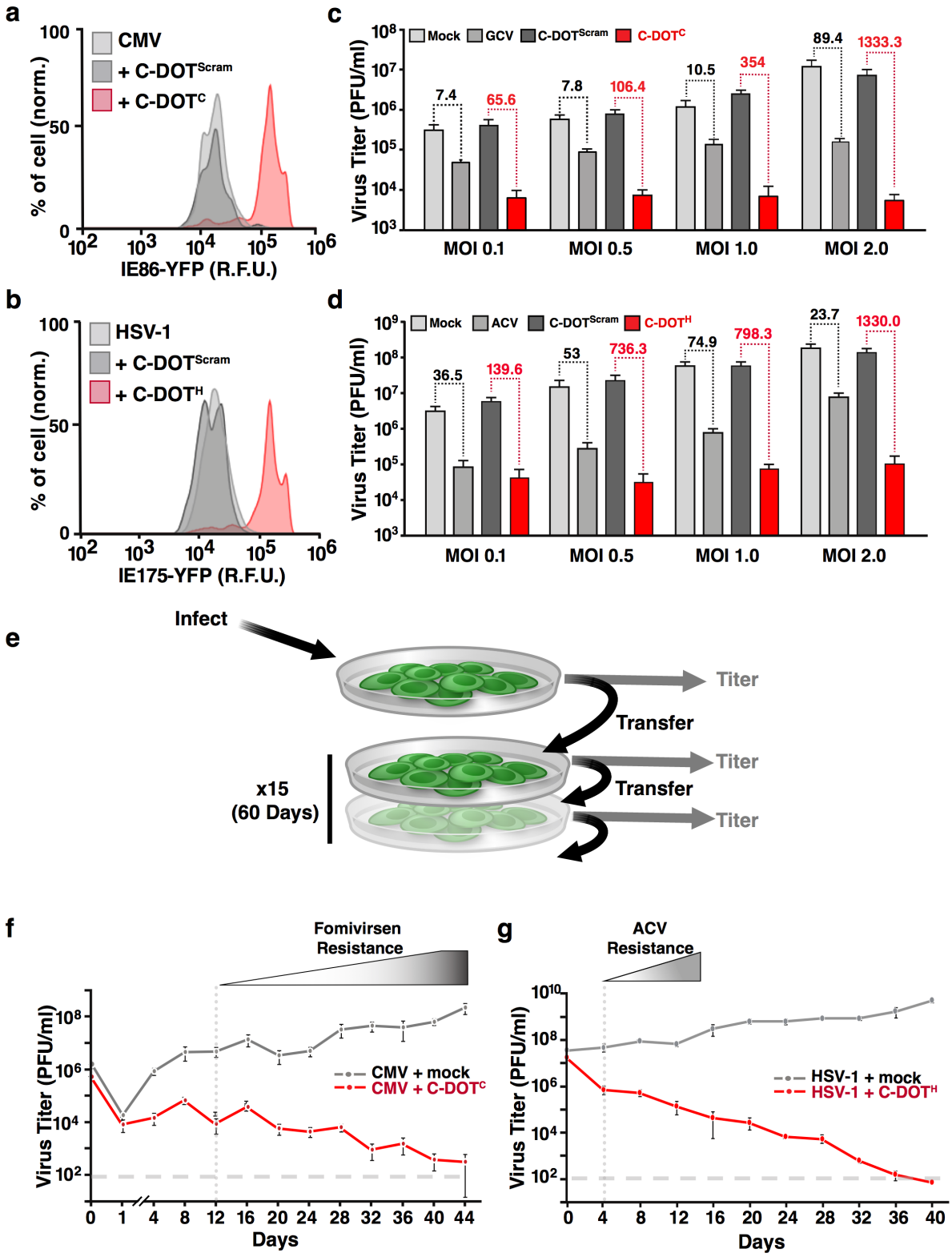

<u>Figure 4:</u> Feedback disruption inhibits viral replication in an *in vivo* model. (a) Schematic of the HSV-1 corneal infection model in mice. BL-6 mice, 6-10 weeks old, undergo corneal debridement followed by infection with HSV-1 17syn+ IE175-YFP virus ($1x10^5$ PFU). 6 hours post infection, 25μM C-DOT^{H}, or C-DOT^{Scram}, or PBS, was topically applied to the cornea. Corneas were harvested at 2 days post infection, imaged for YFP, HSV-1 levels quantified by virus titering, and viral genomes quantified by qPCR. (b) Representative YFP-fluorescence images of corneas after harvesting (nuclei stained with DAPI). (c) Quantification of HSV-1 YFP expressing cells in corneas, as determined from the YFP:DAPI ratio. 5 corneas imaged per sample. (d) HSV-1 viral titers from HSV-1 infected corneas 2 days after treatment with either 25μM PBS, C-DOT^{Scram} or C-DOT^{H}. Corneas were dissociated using collagenase, subjected to three freeze-thaw and supernatant was used to titer virus using end time dilution method (TCID50). Each data point represents a pooling of corneas from three mice (i.e., 9 corneas per treatment). (e) HSV-1 viral genomic DNA quantification by qPCR 2 days after treatment. Each data point represents a pooling of corneas from three mice (i.e., 9 corneas per treatment). p-values less than 0.05 were considered statistically significant: *<0.05, **<0.01, ***<0.001.

Figure 4 (Chaturvedi et al.)

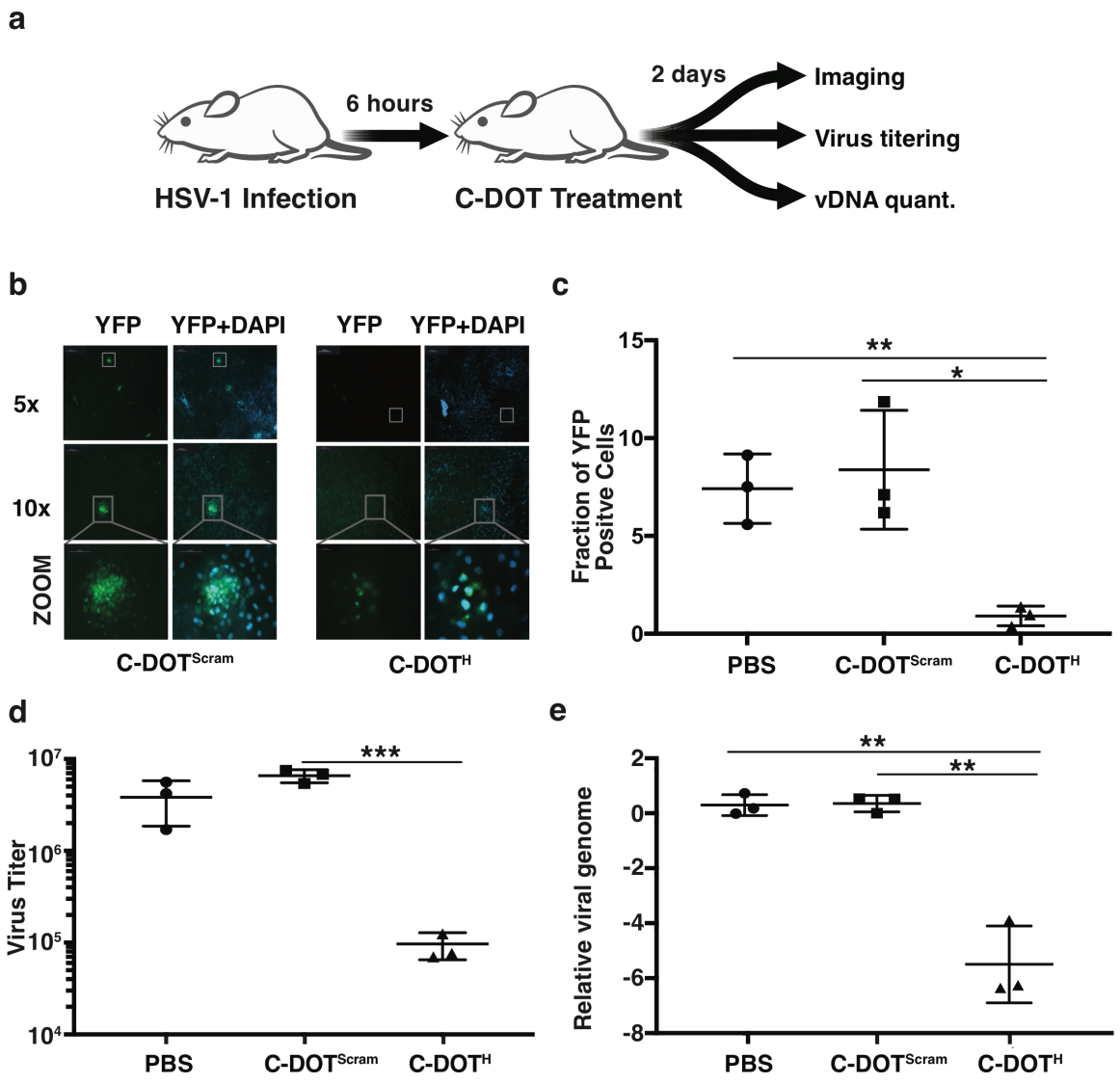

MATERIAL AND METHODS

Mathematical Modeling and Numerical Simulations

We used an experimentally validated ODE model of the CMV IE86 negative feedback circuit[22, 24] modified to include state variables for free crs DNA oligomers (*C-DOTs*) and the IE86–C-DOT bound complex (*BC)*:

$$\boldsymbol{eq.1} \quad \frac{d[IE86]}{dt} = \alpha_0 + \frac{\alpha_1 {k_1}^{h_1}}{[IE86]^{h_1} + {k_1}^{h_1}} + h_1 k_{-2}[BC] - h_1 k_2 [IE86]^{h_1}[CDOT] - \gamma_1 [IE86]$$

$$\boldsymbol{eq.2} \quad \frac{d[CDOT]}{dt} = k_{-2}[BC] - k_2 [IE86]^{h_1}[CDOT]$$

$$\boldsymbol{eq.3} \quad \frac{d[BC]}{dt} = k_2 [IE86]^{h_1}[CDOT] - k_{-2}[BC]$$

where α_0 represents the basal IE86 expression rate (2 unit/hr), α_1 represents the IE86 negative-feedback gain constant (10 unit/hr), h_1 represents the IE86 cooperativity index (hill coefficient), k_1 represents a Michaelis constant (set to 1) for IE86 feedback, γ_1 represents the per-capita IE86 protein degradation rate (0.23 hr^{-1}), k_2 represents the BC dissociation rate (2 hr^{-1}), and k_{-2} represents the BC association rate (1 $unit^{-\eta 1} * hr^{-1}$). In this model, the IE86 can oligomerize ($h_1 \sim 6$)[22] to bind either the crs in its own promoter (MIEP)—thereby mediating negative feedback and down-regulating its own expression rate—or can bind the crs in C-DOT DNA oligo, thereby sequestering IE86 that might otherwise downregulate its own expression via negative feedback. For both binding events, IE86 can transition between free and oligo-bound states but the negative feedback bound state is not explicitly modeled for parsimony and to not introduce unnecessary parameters. The DNA oligonucleotides were assumed to be stable (i.e., not degrade) over the course of the simulation time (validated below). For Extended Data Fig. 1, the initial levels of C-DOT at time=0 were varied as indicated, all other initial conditions were zero. The ODEs were numerically solved using Matlab™.

For calculations of the time to emergence of escape mutants, we utilized an analytic approach[7] previously used to calculate fitness differences between viral strains in patients and the time to emergence of GCV-resistant mutants. Briefly, the equation $s = \frac{1}{t} \ln \left[\frac{q(t)\, p_0}{p(t) q_0}\right]$ describes the relative

fitness, s, of the population and assumes replication occurs in continuous time. The time dynamics of the proportions of most and least fit viral variants (p and q), can be calculated given initial p_0, q_0, and s, (measured at 5.6% for GCV-resistant virus[7]. The mutant arisal time (defined as the time when p(t)=q(t)) can be calculated by algebraic rearrangement $t_{mut} = \frac{1}{s}\ln\left[\frac{1-\mu}{\mu}\right]$. The μ value for TK[8] generates a $t_{mut} \sim 100$ days as observed in the clinic[7]. To predict the time to arisal for a putative C-DOT mutant that has only two single-point mutations (one in IE86 and one in the MIEP region), $t_{mut} = \frac{1}{s}\ln\left[\frac{1-\mu^2}{\mu^2}\right]$, where μ for IE86 and the MIEP region are taken from[9]. The further maximally conservative assumption is made that *s* for C-DOT escape mutants is the same as for TK-escape mutants (in reality, *s* for C-DOT mutants is far lower as it must account for the single mutants that have a 100-fold fitness cost both in presence and absence of C-DOTs).

Protein expression, EMSA and DNA binding assays

BL21 competent *E. Coli* cells (New England Biolabs Inc) were transformed with a pMALcXS plasmid encoding the C-terminus part of IE86 fused to the maltose binding protein, as described[36], and induced with isopropyl b-D thiogalactoside (IPTG) in 1L luria broth (Thermofisher Scientific) containing ampicillin (Sigma-Aldrich). Cells were pelleted at 10,000 RPM for 30 minutes at 4°C and resuspended in 40mL lysis buffer (20mM HEPES, pH 7.4, 1M NaCl, 1mM EDTA, 1mM DTT, Roche protease inhibitor cocktail). Lysozyme was added at a final concentration of 1mg/ml and cells were incubated on ice for 30 minutes, followed by addition of 1mM PMSF and sonication on ice (sonicator at 40% amplitude, 10 seconds on, 30 seconds off-6 repeats). 1mM $MgSO_4$, 0.1mg/ml DNAse (Sigma-Aldrich, St Louis, MO) and 25U/ml Benzonase (Sigma- Aldrich) were then added, cells further incubated on ice for 15-30 minutes, centrifuged at 12,000 rpm for 30 minutes at 4°C and the supernatant incubated with amylose resins (Sigma-Aldrich, St Louis, MO) for 2 hours at 4°C with gentle agitation. Batch bound resin was poured into a column and washed with 10 column volumes of lysis buffer, and eluted in elution buffer (20mM HEPES, pH 7.4^{o}C, 250mM NaCl, 10mM Maltose, 1mM EDTA and 1mM DTT). The eluted protein was passed through a Superose 6 column (GE Healthcare Life Sciences) using gel filtration buffer (20mM HEPES, pH 7.4, 250mM NaCl and 1mM DTT) and used for EMSA or for binding assays. Briefly, digoxygenin labeled oligo probe was made using sequences for crs and Δcrs (see Extended Data Table 1) as

described previously[36]. Binding assays were performed by incubating dsDNA oligonucleotides of various lengths with purified MBP-IE86 for 30 minutes at room temperature and running on Superpose-6 column in the presence of gel filtration buffer and monitored oligomerized form of MBP-IE86 (at 13ml column volume on FPLC) in the presence of different sizes of C-DOT^{C}. To verify the sequence specific interaction between crs and MBP-IE86, EMSAs were performed using the DIG gel-shift kit, 2nd generation (Sigma-Aldrich) according to the manufacturer's instructions. DNA oligonucleotides were obtained from Integrated DNA Technologies (San Jose, CA) (see Extended Data Table 1 for sequences) and resuspended in annealing buffer (100mM Potassium acetate; 30mM HEPES, pH 7.5). Oligonucleotides of complimentary sequences were mixed in equimolar amount, heated to 95°C for 2 minutes, and gradually cooled to 25°C over 45 minutes in a S1000 Thermocycler (Bio-Rad) and stored at –20°C.

Cell-culture conditions and flow cytometry

ARPE-19 cells were maintained in a 1:1 mixture of Dulbecco's Modified Eagle's Medium (DMEM)/F-12 (Mediatech Inc.) with 10% fetal bovine serum (FBS) (HyClone) and 50U/ml Penicillin-Streptomycin (Mediatech Inc.) at 37°C and 5% CO_2 in a humified incubator. MRC-5 fibroblasts, NIH 3T3 mouse fibroblast and Telo-RF were maintained in DMEM with 10% FBS and 50U/ml Penicillin and Streptomycin (Mediatech Inc.). Fomivirsen (NIH), Ganciclovir and Acyclovir (Sigma-Aldrich, St Louis, MO) were added to media at the indicated concentrations following virus inoculate removal. The ARPE-19 stably expressing the MIEP-IE86-GFP minimal circuit were previously described[22]. ARPE-19, Telo-RF (telomerase life extended rhesus fibroblast), NIH 3T3 mouse fibroblast and MRC-5 cell lines were obtained from ATCC. Flow cytometry was performed on BD FACS-Calibur (BD, Biosciences) at the Gladstone flow cytomtery core and analyzed suing FlowJo™ (FlowJo, LLC).

Western blot analysis

10^6 ARPE-19 cells were centrifuged at 2,000g for 10 min at 4°C and resuspended in PBS (Sigma-Aldrich, St Louis, MO). Cells were pelleted, resuspended in ice-cold RIPA lysis buffer (Sigma-Aldrich, St Louis, MO) by vortexing and incubated at 4°C for 30 min. The lysed samples were then pelleted at 13,000 rpm for 20 min at 4°C and supernatants were assayed by western blot as

previously described[24]. Briefly, 20µg of cell lysate total protein was added to 1x loading buffer (100mM Tris-HCl (pH6.8), 200mM DTT, 4% SDS, 0.1% Bromophenol blue, 20% glycerol), and boiled for 10 minutes at 95°C. The lysed samples and precision plus kaleidoscope prestained protein marker (Bio-Rad) were then loaded on 10% Mini-PROTEAN TGX precast protein gel (Bio-Rad) in duplicate and ran at 90V for 2 hours in Tris-glycine running buffer (925mM Tris, 250mM Glycine and 0.1% SDS). One gel was stained for two hours at room temperature with coomassie blue stain (1g coomassie brilliant blue (Bio-Rad), Methanol (50%[v/v]), Glacial acetic acid (10%[v/v]), final volume to 1L with Milli-Q H_2O, followed by destaining (40% methanol, 7% acetic acid in final volume of 1L in Milli-Q H_2O. The gel was blotted on a PVDF membrane using a semi-dry transfer unit (Trans-Blot Semi-Dry Electrophotetic transfer cell, Bio-Rad) at 25V for 45 minutes. The membrane was blocked with Li-Cor Odyssey™ blocking buffer for 2 hours at room temperature with gentle agitation. IE86 protein was detected by a 2-hour incubation of the membrane with an anti-IE86 antibody (1:100 dilution, Mab 810, Chemicon) in Li-Cor Odyssey™ blocking buffer at room temperature followed by 3 5-minute wash steps (1x PBS + 0.01% Tween-20). The membrane was then incubated with a secondary Li-Cor detection antibody (1:20,000 dilution, goat anti-mouse 800CW) for 1 hour in the dark, washed three times in wash buffer (1x PBS + 0.01% Tween-20) and imaged on an Odyssey system (Li-Cor).

Viral Replication Kinetics

The CMV TB40E-IE86-YFP virus was previously described[24] and CMV AD169, GDGrK17, CMV GDGrP53, CMV 759rD100-1, CMV PFArD100 were obtained through the NIH AIDS Reagent Program. MCMV strain K181[37] was kindly provided by Lewis Lanier (UCSF) and Rhesus CMV 68.1 EGFP virus[38] was kindly provided by Peter Barry, UC-Davis. The clinical strain of HSV-1 17syn+ IE175-YFP[39] was kindly provided by Roger Everett, MRC Virology Unit, Glasgow, Scotland that was passaged originally from a clinical isolate[40]. $1x10^6$ ARPE-19 cells were nucleofected with C-DOT^C, C-DOT^H or C-DOT^{Scram} using Amaxa nucleofector (Lonza). 24 hours post-nucleofection cells were infected in triplicate with 0.1 MOI of CMV (TB40E IE86-YFP) or HSV-1 (17syn+ IE175-YFP). Four days post infection, cells were harvested and subjected to three freeze-thaw cycles and used for 10-fold serial dilution titration on naïve ARPE-19 cells. As similar protocol was used to nucleofect MRC-5 cells prior to infection with AD169 and titration

on naïve MRC-5 cells. Titration results were converted to PFU/ml using median tissue culture infectious dose (TCID50)[41]. Similarly, corneal tissues were dissociated using collagenase I (Sigma-Aldrich, St Louis, MO) for 30 minutes, subjected to three freeze-thaw cycles and used for TCID50 analysis.

qPCR, flow cytometry and fluorescent microscopy

Genomic DNA from CMV or HSV-1 infected ARPE-19 cells or mouse corneal tissue dissociated with collagenase I for 30 minutes was extracted using DNeasy Blood and tissue kit (Qiagen). TLR9 expression analysis was performed by total cell RNA extraction using an RNEASY RNA isolation kit (74104; QIAGEN) and reverse transcription using a QuantiTet Reverse Transcription kit (205311; QIAGEN). Relative quantification of genomic DNA or cDNA was performed on a 7900HT Fast Real-Time PCR System (ThermoFisher Scientific, 4329003) using sequence specific primers (Extended Data Table 1) and Fast SYBR Green Master Mix (Applied Biosystems, 4385612). To measure the mean fluorescent intensity of YFP, flow cytometry was performed on trypsinized cells using BD FACS Calibur (BD Biosciences). Fluorescent microscopy of the cornea infected with HSV-1 was performed using Leica Zeiss fluorescent microscope for DAPI (excitation at 345nm) and YFP (excitation at 514 nm). Images were analyzed using Image J software at threshold 100 for DAPI and YFP mask images, followed by particle analysis at size 2 micron^2 for YFP and 10micron^2 for DAPI.

Corneal infection assays in mice

All experiments were performed with 6- to 10-week old male and female sibling Black 6 mice. Breeding pairs were purchased from Jackson laboratories (Bar Harbor, Maine) and maintained under pathogen-free conditions in the UCSF barrier facility. All animal experiments were conducted in accordance with procedures approved by the UCSF Institutional Animal Care and Use Committee. Corneal epithelial debridement was performed on mice as previously described[42]. Briefly, mice were anesthetized by isofluorane inhalation (Abbott Laboratories, Alameda, CA). The central part of the epithelium was removed down to the basement membrane using an Algerbrush II (Katena Products, Inc., Denville, NJ). 5µl of HSV-1 17syn+ YFP-IE175 (10^5 pfu) were immediately applied to the debrided cornea. 6h later, mice were anesthetized again and 5µl

of C-DOT^{H}, C-DOT^{scram} or PBS were applied to the cornea for 5 min. At the indicated time post infection, eyes were enucleated and the corneas were dissected to remove the lens, iris, and retina. Four incisions were made equal distances apart to aid in flattening the corneas. Fresh corneas were counterstained using 0.5µg/ml DAPI, mounted on slides with Fluoro-gel (Electron Microscopy Sciences, Hatfield, PA) and imaged using Leica Zeiss Confocal microscopy. Corneas were dissociated using collagenase I (Sigma-Aldrich, St Louis, MO), total DNA was extracted using DNeasy Blood & Tissue kit (QIAGEN), and subjected to qPCR using Fast SYBR green master mix (4385612; Applied Biosystems), analyzed on a 7900HT Fast Real-Time PCR System (4329003; Thermofisher Scientific). Virus titer was determined as described above.

Statistical analysis

Statistical differences were determined by using the two-tailed unpaired Student's *t* test (GraphPad Prism, La Jolla, CA). A p-value less than 0.05 was considered statistically significant: *<0.05, **<0.01, ***<0.001, ****<0.0001, ns: not significant.

Oligonucleotide preparation, modification, and nanoparticle construction

C-DOT^{C}, C-DOT^{H}, C-DOT^{MCMV,} C-DOT^{RhCMV}, cy3- C-DOT^{C} were made by annealing sequence specific oligonucleotides (see Extended Data Table 1 for sequences). Briefly, DNA oligonucleotides were obtained from Integrated DNA Technologies (San Jose, CA) and resuspended in annealing buffer (100mM Potassium acetate; 30mM HEPES, pH 7.5). Oligonucleotides of complimentary sequences were mixed in equimolar amount, heated to 95°C for 2 minutes, and gradually cooled to 25°C over the period of 45 minutes in a S1000 Thermocycler (Bio-Rad) and stored at –20°C. Spherical nucleic acids (cy3-C-DOT^{C}-SNA) were made using 3' thiol labeled C-DOT^{C} forward strand and 5' cyanine 3- phosphoramidite (cy3) tagged reverse strand oligo obtained from Bioneer, Inc (Alameda, CA) (see Extended Data Table 1 for sequences). Oligonucleotides were annealed as mentioned above and cy3-C-DOT-SNA were made as described previously[43]. Briefly, annealed oligonucleotides were added to 10nm citrate stabilized gold nanoparticle (Sigma-Aldrich, St Louis, MO) (~3nmol oligonucleotide per 1ml of 10nM colloid). After 20 minutes, 10% SDS (Sigma- Aldrich, St Louis, MO) was added to bring down the concentration of SDS to 0.1% in phosphate buffer (0.01M, pH 7.4). 2.0M NaCl was then added

to bring salt concentration to 0.1M. Oligonucleotides were incubated under shaking conditions at room temperature for 30 min, followed by two successive additions of 2.0M NaCl at 30-minute interval to bring the final concentration of NaCl to 0.3M. The final mixture was incubated under shaking conditions to complete the functionalization of oligonucleotides on gold nanoparticles. The cy3-C-DOT-SNA was recovered by three centrifugation steps (13,000 rpm, 20 minutes), resuspended in 1x PBS buffer and stored at $4^{o}C$ until used.